JACS
JOURNAL OF THE AMERICAN CHEMICAL SOCIETY
Article
pubs.acs.org/JACS

Gas-Phase Reactivity of Group 11 Dimethylmetallates with Allyl Iodide

Nicole J. Rijs,[†,‡,§] Naohiko Yoshikai,[∥] Eiichi Nakamura,[⊥] and Richard A. J. O'Hair*[,†,‡,§]

[†]School of Chemistry, and [‡]Bio21 Institute of Molecular Science and Biotechnology, The University of Melbourne, Victoria 3010, Australia

[§]ARC Centre of Excellence for Free Radical Chemistry and Biotechnology

[∥]Division of Chemistry and Biological Chemistry, School of Physical and Mathematical Sciences, Nanyang Technological University, Singapore 637371

[⊥]Department of Chemistry, The University of Tokyo, Bunkyo-ku, Tokyo 113-0033, Japan

Supporting Information

ABSTRACT: Copper-mediated allylic substitution reactions are widely used in organic synthesis, whereas the analogous reactions for silver and gold are essentially unknown. To unravel why this is the case, the gas-phase reactions of allyl iodide with the coinage metal dimethylmetallates, $[CH_3MCH_3]^-$ (M = Cu, Ag and Au), were examined under the near thermal conditions of an ion trap mass spectrometer and via electronic structure calculations. $[CH_3CuCH_3]^-$ reacted with allyl iodide with a reaction efficiency of 6.6% of the collision rate to yield: I^- (75%); the cross-coupling product, $[CH_3CuI]^-$ (24%); and the homo-coupling product, $[C_3H_5CuI]^-$ (1%). $[CH_3AgCH_3]^-$ and $[CH_3AuCH_3]^-$ reacted substantially slower (reaction efficiencies of 0.028% and 0.072%). $[CH_3AgCH_3]^-$ forms I^- (19%) and $[CH_3AgI]^-$ (81%), while only I^- is formed from $[CH_3AuCH_3]^-$. Because the experiments do not detect the neutral product(s) formed, which might otherwise help identify the mechanisms of reaction, and to rationalize the observed ionic products and reactivity order, calculations at the B3LYP/def2-QZVP//B3LYP/SDD6-31+G(d) level were conducted on four different mechanisms: (i) S_N2; (ii) S_N2'; (iii) oxidative-addition/reductive elimination (OA/RE) via an M(III) η^3-allyl intermediate; and (iv) OA/RE via an M(III) η^1-allyl intermediate. For copper, mechanisms (iii) and (iv) are predicted to be competitive. Only the Cu(III) η^3-allyl intermediate undergoes reductive elimination via two different transition states to yield either the cross-coupling or the homo-coupling products. Their relative barriers are consistent with homo-coupling being a minor pathway. For silver, the kinetically most probable pathway is the S_N2 reaction, consistent with no homo-coupling product, $[C_3H_5AgI]^-$, being observed. For gold, no C−C coupling reaction is kinetically viable. Instead, I^- is predicted to be formed along with a stable Au(III) η^3-allyl complex. These results clearly highlight the superiority of organocuprates in allylic substitution reactions.

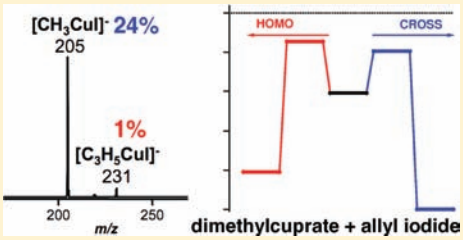

INTRODUCTION

Copper-mediated allylic substitution reactions, Scheme 1, are both synthetically useful and most interesting from a mechanistic viewpoint.[1] Corey and Posner first reported stoichiometric reactions between cuprates and allylic substrates in the late 1960s in their classic exploration of C−C coupling reactions with Gilman reagents,[2] and Rona et al. employed the reaction for the synthesis of steroid derivatives.[3] A major research front in the past two decades has been the development of diastereoselective and enantioselective catalytic variants.[1d,e,4] These have been used as key steps in a number of synthetic applications[5] including the synthesis of a butenolide natural product[5a] and in the formal synthesis of (−)-naproxen.[5b]

One of the most fascinating aspects of these "allylic alkylation" reactions is that they exhibit a range of chemo-, regio-, and stereoselectivities.[1] With regards to regioselectivity, attack by the nucleophilic carbon can occur at the α carbon to give product **1**, or at the γ carbon to give product **2** (Scheme 1).

A key challenge in developing robust and predictable copper-mediated allylic alkylation reactions is that the relationship between the copper reagent (e.g., structure, cluster size, nature of auxiliary ligand (L), overall charge, etc.), the allylic substrate, and the reaction medium (solvent, counterions etc) is often poorly understood. Thus, in many synthetic studies, (i) ill-defined reagents are used, and (ii) only the final organic product(s) are isolated and characterized. Mechanistic insights into these reactions have been hard won through the use of theoretical calculations,[6,7] and in rare instances, NMR has been used to examine the intermediates and products of organocuprate reactions with allylic substrates.[8]

The generally accepted mechanism for copper-mediated allylic alkylation reactions is shown in Scheme 2. It involves

Received: July 28, 2011
Published: January 26, 2012

   dx.doi.org/10.1021/ja2069032 | J. Am. Chem.Soc. 2012, 134, 2569−2580

Scheme 1. Allylic Alkylation Reactions of Organocopper Complexes[a]

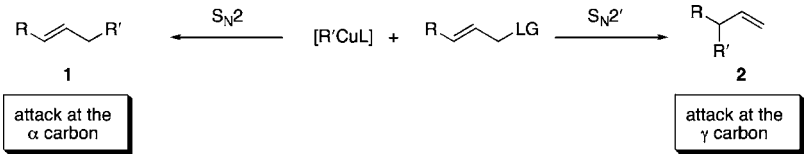

[a]L = ligand(s); LG = leaving group.

Scheme 2. Suggested Mechanism of Copper-Mediated Allylic Alkylation Reactions

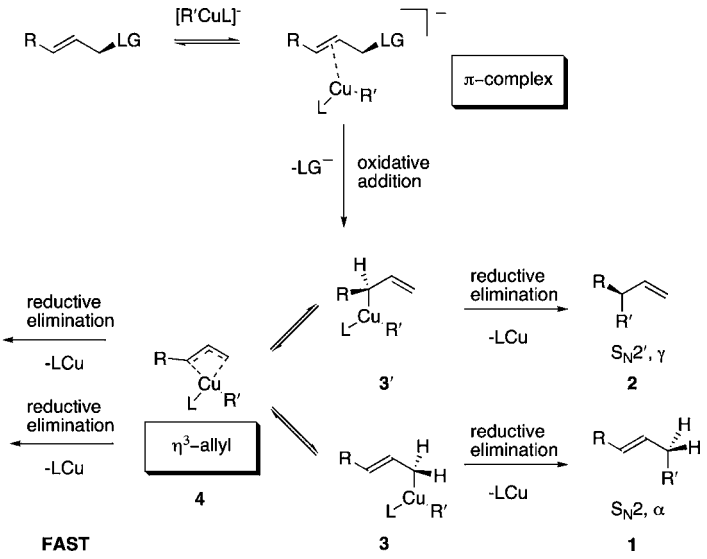

Scheme 3. Substrate-Directed Outcomes in Reactions of Organocuprates with Allyl Halides: (A) Cross-Coupling versus Homo-Coupling Products; (B) Formation of Cu^{III} Complexes, η^3-Allyl versus Tetramethylcuprate

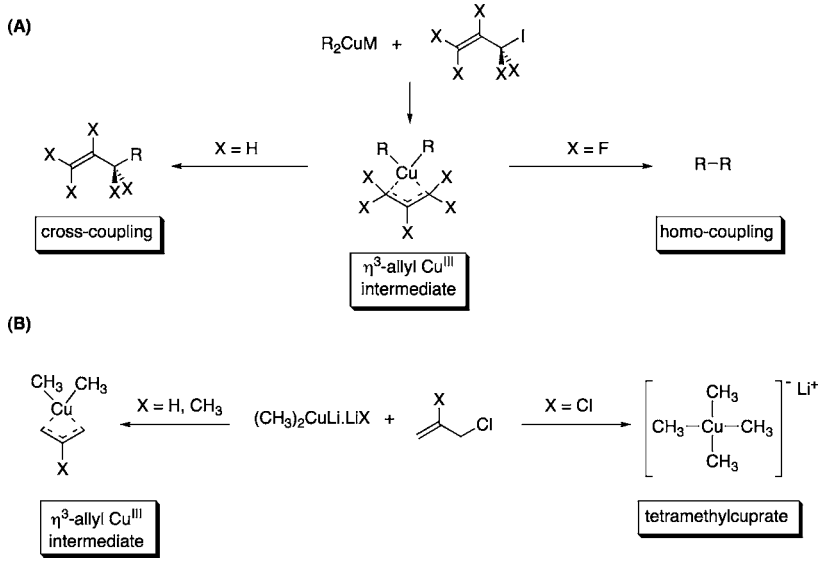

oxidative addition of the substrate to the organocuprate complex, which takes place with *anti*-stereochemistry. This oxidative addition may be regioselective depending on the ligands. For example, if a heterocuprate bearing a less σ-donating ligand such as CN^- is used, then the reaction is γ-selective.[7e] Isomerization between η^1-allyl intermediates **3** and **3′** at the α- and γ- positions can proceed via the η^3-allyl intermediate, **4** (Scheme 2). If the α- and γ-carbons have different substituents and are nonequivalent (e.g., R ≠ H in Scheme 2), reductive elimination will occur to a different extent at the α- and γ-positions.[7a] A previous theoretical study has revealed that the barrier for reductive elimination from the η^3-allyl intermediate **4** is lower than those for the η^1-allyl intermediates **3** and **3′**. Thus, **4** is predicted to undergo reductive elimination more rapidly.[7a] Indeed, it is now generally accepted that reductive elimination directly from the η^3-allyl intermediate is the preferred mode of C–C bond coupling.[7a,e,8a]

Despite the use of stoichiometric, "well-defined" reagents, organocuprates continue to yield unexpected results. For

dx.doi.org/10.1021/ja2069032 | J. Am. Chem.Soc. 2012, 134, 2569–2580

example, recent reports have highlighted that the substrate can control the preferred reaction pathway (Scheme 3). Thus, Norinder et al. reported that dialkylcuprates react with allyl iodide via the expected cross-coupling pathway, but that perfluoro allyl iodide exclusively yields the homo-coupling product (Scheme 3A).[7d] More recently, Bartholomew et al. have used NMR to observe the formation of different types of Cu(III) intermediates in the reactions of halo-Gilman reagents with allyl chlorides (Scheme 3B).[8] In their experiments when allyl chloride was used, the η^3-allyl intermediate was observed.[8a] In contrast, when 2,3-dichloropropene was used, tetramethylcuprate was observed.[8b]

Although there is widespread interest in silver and gold-mediated C−C bond-forming reactions,[9] remarkably little is known about their potential in allylic alkylation reactions.[10] To date, there appears to have only been a theoretical report comparing the reactions of allylic substrates with all three coinage metal dimethylmetallates.[7b] It was found that $[CH_3AgCH_3]^-$ does not benefit from an allylic π-interaction as effectively as does $[CH_3CuCH_3]^-$, thereby disfavoring reductive elimination. Because of lower lying 5d-orbitals, such a π-interaction is completely absent for $[CH_3AuCH_3]^-$. Thus, the silver and gold dimethylmetallates were theoretically predicted to be less effective reagents for C−C coupling of allylic substrates as compared to copper.

Gas-phase studies represent a powerful way of uncovering the intrinsic reactivity of organometallic ions and the mechanisms of metal-mediated C−C bond-coupling reactions.[11−14] There are several benefits from combining the multistage mass spectrometry (MS^n) capabilities of an ion trap with quantum mechanical calculations.[12] These include:

(i) Fundamental reactivity is probed because the complicating effects of solvent and counterions are absent.

(ii) Gronert's pioneering studies on the temperature of ions trapped in an ion trap mass spectrometer without ion activation have shown that their temperatures are at near thermal conditions (i.e., room temperature).[15] Furthermore, the organometallates $[CH_3MCH_3]^-$ (where M = Cu, Ag, and Au) can be isolated and stored in an ion trap mass spectrometer for 10 s without any decomposition.[16] In fact, these ions only undergo fragmentation when subjected to collisional activation.[17,16d] This contrasts with solution, where organocuprates are only stable over a narrow temperature range (typically well below room temperature), and can readily undergo decomposition above these temperatures.[18]

(iii) The desired ionic organometallic reactant can be confidently assigned via the unique mass and often-distinctive isotopic signature of the metal. It can then be mass-selected using well-established tandem mass spectrometry-based approaches,[19] and its reactivity can be directly probed by monitoring the changes in its abundance as well as the formation of ionic products.[12] This contrasts with solution, where the reactive species is generally not easily isolated and characterized. Because many stoichiometric organometallic reagents are prone to forming oligomeric species, the relationship between oligomeric structure and reactivity is often poorly understood.[20,21]An even worse scenario can occur for metal-catalyzed reactions, where trace metal impurities may be the actual catalysts. Recent examples in metal-catalyzed cross-coupling reactions have highlighted that copper impurities may be the reactive catalyst rather than iron,[22] and palladium impurities may be responsible for gold(I) Sonogashira coupling.[23] These important issues are thus circumvented in gas-phase studies.

(iv) In multistage mass spectrometry experiments, the ionic reactants are directly linked to the ionic products and there are no solvent molecules. This narrows the scope of theoretical calculations to be performed. This contrasts with theoretical studies based on condensed phase data, where crystal structures of the organometallic species and the nature of the isolated organic product(s) are used to guide theory, and where the role of solvent molecules needs to be explored.

Previous studies have focused on the gas-phase chemistry of two classes of organo-coinage ions, both formed via decarboxylation reactions of appropriate precursor ions:[16,24−26] (i) dimethylmetallates, $[CH_3MCH_3]^-$ (M = Cu, Ag, and Au), which are directly related to "Gilman" reagents;[16d,27] and (ii) alkyl metal cluster cations, $[CH_3M_2]^+$ (M = Cu and Ag).[28] For the anionic systems, dimethylcuprate was observed to promote carbon−carbon bond formation in ion−molecule reactions with methyl iodide, while dimethylargentate and dimethylaurate did not.[16d,27] For the cationic systems, both $[CH_3Cu_2]^+$ and $[CH_3Ag_2]^+$ were shown to undergo carbon−carbon bond formation with allyl iodide.[28]

Here, a combination of mass spectrometry-based experiments and electronic structure calculations is used to examine the gas-phase reactivity and mechanisms of coinage metal-mediated allylic alkylation reactions between dimethylmetallates and allyl iodide.

EXPERIMENTAL SECTION

Reagents. Gold(III) acetate was obtained from Alfa Aesar. Allyl iodide, methyl iodide, sodium bromide, copper(II) acetate, and silver(I) acetate were obtained from Aldrich. Acetic acid-d_4 was obtained from Cambridge Isotope Laboratories. All chemicals were used without further purification.

Mass Spectrometry. Ion−molecule reactions were performed on a modified Finnigan LCQ quadrupole ion trap mass spectrometer equipped with a Finnigan ESI (electrospray ionization) source, as previously described.[29] Methanolic solutions of metal acetate with concentrations of 0.5−1.0 mM were injected into the ESI source at a flow rate of 5 μL/min. The gold(III) acetate methanol solution was acidified with acetic acid and chilled, but decomposed at a moderate rate, and therefore dilution followed by immediate electrospray was required. Typical electrospray source conditions involved needle potentials of 3.5−4.5 kV and a heated capillary temperature of 180 °C. Mass selection, collisional activation, and ion−molecule reactions were carried out using the "advanced scan" function of the LCQ software, which allows the Q value and the reaction time to be varied. The neutral substrate allyl iodide was introduced at various concentrations into the ion trap via the helium inlet line. Rates were measured by varying the time delay between isolation of the $[CH_3MCH_3]^-$ (M = Cu, Ag, and Au) reactant ion and its mass analysis ("reaction delay", RD). The decay of $[CH_3MCH_3]^-$ was monitored over at least six values of RD. The intensity of the reactant ion was calculated by integration of its ion count within the mass-selected window. Pseudo first-order rates were estimated by extrapolation of plots of $-\ln([CH_3MCH_3]^-$ intensity/total ions) versus RD. Rate constants were calculated by dividing the pseudo first-order rate coefficient by the calculated concentration of allyl iodide in the ion trap. The rate constants reported are the average of at least nine independent measurements conducted on at least three separate days.[30] Standard deviations in rate constants were typically around 7% for M = Cu, 40% for M = Ag, and 20% for M = Au, larger for the latter two metals as a result of much slower reaction rates. A conservative estimate of error is

dx.doi.org/10.1021/ja2069032 | J. Am. Chem.Soc. 2012, 134, 2569−2580

Scheme 4. Generation and Gas-Phase Bimolecular Reaction of Organometallates

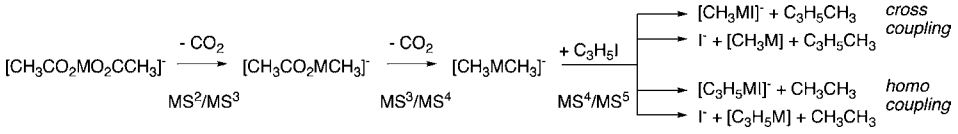

±25%, but relative rates are expected to be more accurate due to cancellation of errors.

Theoretical Calculations. Theoretical calculations were carried out to provide insights into the bimolecular reactivity of the dimethylmetallate anions. Gaussian 03,[31] utilizing the B3LYP hybrid functional,[32] was used for all geometry optimizations and vibrational frequency calculations. The Stuttgart Dresden (SDD) basis set and effective core potential (ECP) were used for the copper, silver, gold, and iodine atoms, while the 6-31+G(d) all electron basis set was used for carbon and hydrogen.[33] This combination was chosen because (i) it has been shown to be effective in calculating organometallate systems while being less demanding than higher levels of ab initio theory;[34] and (ii) to allow comparison with previous work.[16d]

Optimized B3LYP geometries of the metalate complexes were previously compared to those determined from X-ray crystallography.[16b−d,34] There was excellent structural agreement between the calculated geometries and those determined experimentally.[35]

All transition state (TS) geometries were characterized by the presence of a single imaginary frequency, and intrinsic reaction coordinates (IRC) were examined to ensure smooth connection of reactants and products.

Single point energies calculated with successively more complete basis sets (Supporting Information Tables S1−S4) did not alter the relative ordering of predicted energetic pathways. Energetics presented were calculated with B3LYP utilizing the Def2-QZVP basis set (C, H = all electron; Cu, Ag, Au, and I = incl. ECP),[36] defined as B3LYP/Def2-QZVP//B3LYP/SDD6-31+G(d). All quoted relative energies (E_0) include zero-point vibrational energy (unscaled) calculated at the optimization level, without correction for basis set superposition error.

To assess the robustness of the B3LYP results, key stationary points were calculated with the M06 functional[37a] and the B2PLYPD double hybrid functional[37b,c] (Supporting Information Tables S6−S17). For the copper system, the predicted energetic trends are entirely consistent between all three methods. The energetic results for silver and gold also are in agreement with the comparative lack of reactivity of these systems. Discussion of these results is available in the Supporting Information (p S38).

Visualizations of the molecules appearing in this Article were created using MacMolPlt.[38]

Collision rates were calculated via the Average Dipole Orientation (ADO) theory of Su and Bowers using the COLRATE program.[39]

RESULTS AND DISCUSSION

1. Experimental Reactivity of Allyl Iodide with Coinage Metal Dimethylmetallates. Organometallate precursor ions were generated via multistage mass spectrometry methods using a double decarboxylation strategy. Decarboxylation was induced by collisional activation (Scheme 4). As this process has been described in detail in previous reports,[16,27] here the focus is on the bimolecular reactivity of the organometallates with allyl iodide (MS^4 experiments for M = Cu, Ag; MS^5 experiments for M = Au).

1.1. Experimental Reactivity of Allyl Iodide with Dimethylcuprate. Ion molecule reactions (IMR) were conducted between the dimethyl cuprate anion (m/z 93) and allyl iodide (Scheme 4, MS^4 experiment). An examination of Figure 1a reveals the formation of three primary product ions: I^- (m/z 127), $[CH_3CuI]^-$ (m/z 205), and $[C_3H_5CuI]^-$ (m/z 231). In addition, $[ICuI]^-$ m/z 317 is observed, the product of a secondary reaction, as confirmed by mass isolation and

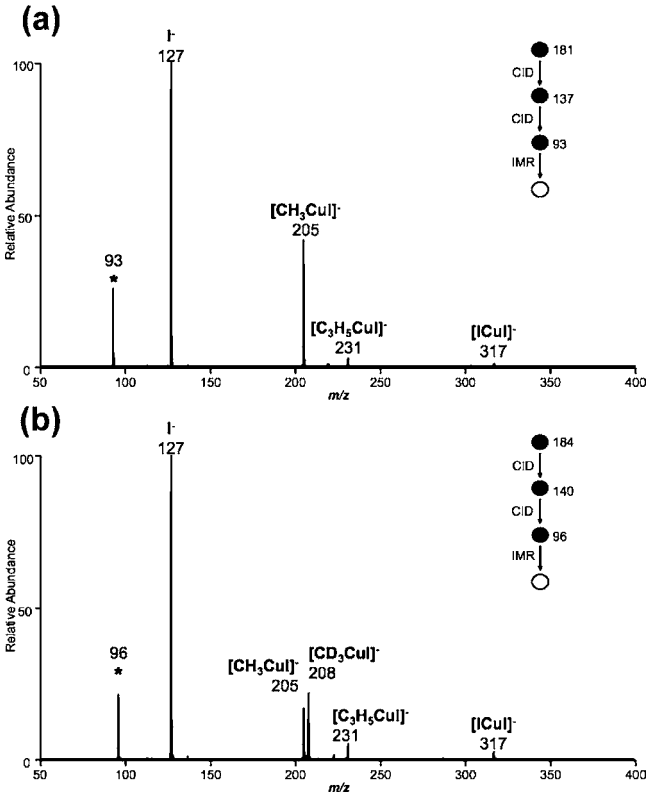

Figure 1. MS^4 mass spectra showing ion molecule reaction between allyl iodide, C_3H_5I, and (a) dimethylcuprate anion $[CH_3CuCH_3]^-$ (m/z 93); (b) deuterated dimethylcuprate anion $[CD_3CuCH_3]^-$ (m/z 96). The mass-selected ion is marked with an "*" in each case.

reaction of $[CH_3CuI]^-$ (data not shown). These assignments were confirmed via the reaction of allyl iodide with the isotopically labeled cuprates $[CD_3CuCH_3]^-$ (m/z 96, Figure 1b) and $[CD_3CuCD_3]^-$ (m/z 99, Supporting Information Figure S1a). The organometallic ions $[CH_3CuI]^-$ and $[C_3H_5CuI]^-$ arise from C−C bond-coupling reactions occurring via cross-coupling and homo-coupling pathways, respectively (Scheme 4, where M = Cu).

The kinetics and branching ratios for the reaction of $[CH_3CuCH_3]^-$ with allyl iodide are summarized in Table 1. The rate of reaction for dimethylcuprate and allyl iodide was found to be 8.63×10^{-11} cm^3 molecules^{-1} s^{-1}, which is more than double the rate for the reaction with CH_3I (3.74×10^{-11} cm^3 molecules^{-1} s^{-1}).[27] The ADO reaction efficiency was 6.6%, corresponding to a reaction occurring approximately once in every 15 collisions. The branching ratios for the primary product ions were determined from plots of the integrated ion intensity as a function of reaction time (Supporting Information Figure S2). The iodide anion is the major product, with a branching ratio of 75%. The cross-coupling product $[CH_3CuI]^-$ is the next most abundant product, with a 24% overall yield. Homo-coupling is found to be a relatively minor pathway in comparison to cross-coupling, with only a 1% yield of $[C_3H_5CuI]^-$.

dx.doi.org/10.1021/ja2069032 | J. Am. Chem.Soc. 2012, 134, 2569−2580

Table 1. Kinetics and Branching Ratios of Ionic Products for the Gas-Phase Ion−Molecule Reactions of Allyl Iodide with Dimethylcuprate, Dimethylargentate, and Dimethylaurate

		$[CH_3CuCH_3]^-$	$[CH_3AgCH_3]^-$	$[CH_3AuCH_3]^-$
rate data	$k_{measured}$	863×10^{-13}[a,b]	3.2×10^{-13}[a,c]	7.4×10^{-13}[a,d]
	k_{ADO}	1.30×10^{-9}	1.16×10^{-9}	1.03×10^{-9}
reaction efficiency[e]		6.6%	0.028%	0.072%
product ion branching ratios	I^- (m/z 127)	75%	19%	>99%
	$[CH_3MI]^-$	m/z 205, 24%	m/z 249, 81%	m/z 339, <1%
	$[C_3H_5MI]^-$	m/z 231, 1%	not observed	not observed

[a] In units of cm^3 molecules^{-1} s^{-1}. [b] $\pm 61 \times 10^{-13}$. [c] $\pm 1.3 \times 10^{-13}$. [d] $\pm 1.6 \times 10^{-13}$. [e] Reaction efficiency = $(k_{measured}/k_{ADO}) \times 100$.

Scheme 5. Possible Mechanistic Pathways for C−C Coupling Reactions

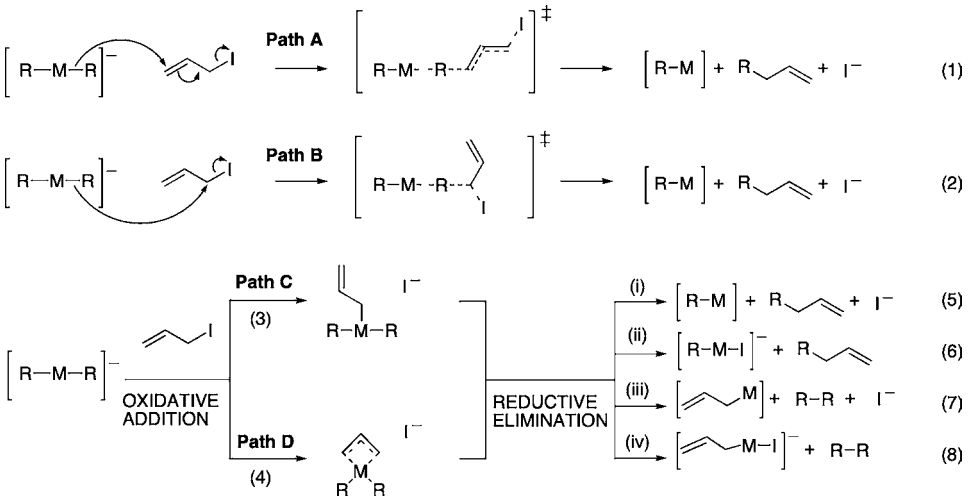

Finally, a secondary deuterium kinetic isotope effect (k_H/k_D) for the cross-coupling channel can be determined by comparing the integrated ion abundances of the product ions $[CD_3CuI]^-$ (m/z 208) and $[CH_3CuI]^-$ (m/z 205). Because this product ion undergoes secondary reactions, the isotope effect was determined at a range of reaction times. Before any significant secondary reaction had occurred, the measured isotope effect is $k_H/k_D = 1.2 \pm 0.1$. This contrasts with the inverse secondary isotope effect $k_H/k_D = 0.82 \pm 0.05$ previously measured in the C−C bond-coupling reaction between $[CD_3CuCH_3]^-$ and CH_3I.[27] While mechanistically complex to interpret, these contrasting isotope effects may reflect different mechanisms for these two reactions.[40]

1.2. Experimental Reactivity of Allyl Iodide with Dimethylargentate and Dimethylaurate. Next, the reactions of mass-selected dimethylargentate and dimethylaurate with allyl iodide were examined (typical spectra are given in the Supporting Information, Figure S1b,c). While there is no evidence of the product arising from homo-coupling, $[CH_3AgCH_3]^-$ reacts with allyl iodide at a rate of 3.2×10^{-13} cm^3 molecules^{-1} s^{-1} (reaction efficiency of 0.028%) to form I^- and the product arising from cross-coupling, $[CH_3AgI]^-$, with branching ratios of 19% and 81%, respectively.[41] This reaction efficiency is around 3 orders of magnitude less than that of the cuprate, corresponding to a reaction in around 1 in every 3600 collisions. $[CH_3AuCH_3]^-$ also reacts slowly with allyl iodide (7.4×10^{-13} cm^3 molecules^{-1} s^{-1}, reaction efficiency 0.072%) to yield I^- (branching ratio >99%). Essentially none of the ionic product associated with cross-coupling, $[CH_3AuI]^-$, is observed (branching ratio <1%). The aurate reaction efficiency is around the same order of magnitude of that of the argentate, corresponding to a reaction once in every 1400 collisions. It is interesting to note that previous studies have shown that $[CH_3AgCH_3]^-$ and $[CH_3AuCH_3]^-$ both are unreactive toward methyl iodide in the gas phase,[16d,27] highlighting the enhanced reactivity of the allylic substrate.

2. Electronic Structure Calculations To Gain Insight into Reaction Mechanisms of Allyl Iodide with Coinage Metal Dimethylmetallates. Scheme 5 summarizes the possible mechanistic pathways: concerted nucleophilic substitution at the S_N2' (path A, γ-carbon) or S_N2 (path B, α-carbon) position; stepwise σ-type oxidative addition (α-carbon) followed by reductive elimination (path C); and stepwise π-type oxidative addition followed by reductive elimination (path D, γ-carbon). Homocoupling (eqs 7 and 8) may only occur via the M(III) intermediate formed in path D as the T-shaped intermediate of path C has both methyl groups in an unfavorable trans relationship.

The experiments highlighted important differences in the reactivity of allyl iodide with the three metallates. However, the mechanisms of reaction remain shrouded due to (i) the fact that neutral products are not detected; thus iodide can be a product of cross-coupling, homo-coupling (Scheme 4), or, more simply, oxidative addition (eqs 3 and 4); and (ii) that there may be more than one mechanism that can give rise to identical coupling products (for example, eqs 1, 2, and 5, Scheme 5). Specifically, $[CH_3MI]^-$ can arise from four different mechanisms: concerted nucleophilic substitution (path A or B, eq 1 or 2) or via reductive elimination after oxidative addition (path C or D, eq 6). By contrast, $[C_3H_5MI]^-$ can only arise from reductive elimination (eq 8) that proceeds from a π-oxidative addition (path D).

dx.doi.org/10.1021/ja2069032 | J. Am. Chem.Soc. 2012, 134, 2569−2580

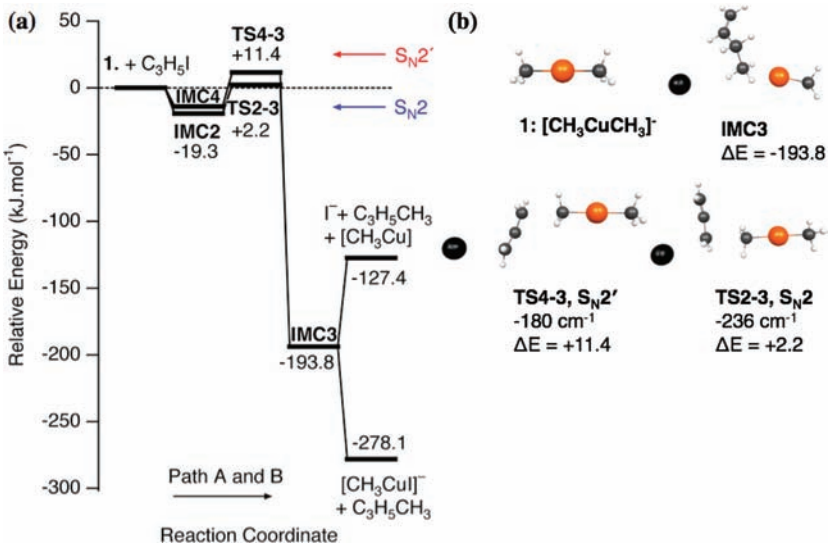

Figure 2. (a) Calculated B3LYP/Def2-QZVP//B3LYP/SDD6-31+G(d) relative energies (kJ mol^{-1}) for minima and transition states relevant to bimolecular reactions of $[CH_3CuCH_3]^-$ + C_3H_5I via paths A and B; and (b) structures of minima and transition states relevant bimolecular reactions of $[CH_3CuCH_3]^-$ + C_3H_5I via paths A and B of Scheme 5.

To establish which of the mechanisms shown in Scheme 5 accounts for the experimentally observed product ions, the next sections report on the predictions of electronic structure calculations.

2.1. Dimethylcuprate Reactivity. The calculated potential energy surfaces for the concerted nucleophilic substitution reactions (Scheme 5, paths A and B) are shown in Figure 2. Although substitution at the S_N2' position (path A) is predicted to be exothermic overall, the activation barrier is above that of the separated reactants (+11.4 kJ mol^{-1}, Figure 2) and thus is not expected to be viable. Substitution via the S_N2 position (path B) has a slightly lower barrier (+2.2 kJ mol^{-1}, Figure 2), consistent with the α-carbon being more electrophillic. These concerted mechanisms alone cannot account for the homo-coupling side product $[C_3H_5CuI]^-$ (Figure 1).

The potential energy diagrams for the oxidative addition/reductive elimination pathways are given in Figures 3 and 4. While the current focus is on iodide-assisted pathways, additional data for reductive elimination pathways in the absence of iodide are shown in the Supporting Information (Figures S8−S11). Because these pathways are found to be higher in energy in all cases, they are not discussed here.

The oxidative addition/reductive elimination pathway proceeding via the η^1-allyl Cu(III) intermediate (Figure 3 and path C, eqs 3 and 5 of Scheme 5) is energetically favored over the S_N2 and S_N2' reactions (Figure 2). The rate-controlling step is oxidative addition (−27.3 kJ mol^{-1}, α-carbon); however, the reductive elimination is similarly high in energy (−37.5 kJ mol^{-1}) as compared to the exit channel (−278.1 kJ mol^{-1}). The reaction is σ-bond oriented, as supported by the linear nature of the transition state (Figure 3b, **TS5−6**, OA_σ), which suggests that the copper d_z^2 orbital is involved in the interaction with the C−I σ^* orbital. Because there is no opportunity for homo-coupling via this η^1-allyl intermediate, path C also cannot account for the formation of $[C_3H_5CuI]^-$.

The alternative oxidative addition/reductive elimination pathway, path D, involving an η^3-allyl Cu(III) intermediate, is shown in Figure 4. The barrier for the π-oxidative addition is lower (−26.0 kJ mol^{-1}) than those of the concerted S_N2 and S_N2' reactions pathways (Figure 2) and is essentially equivalent

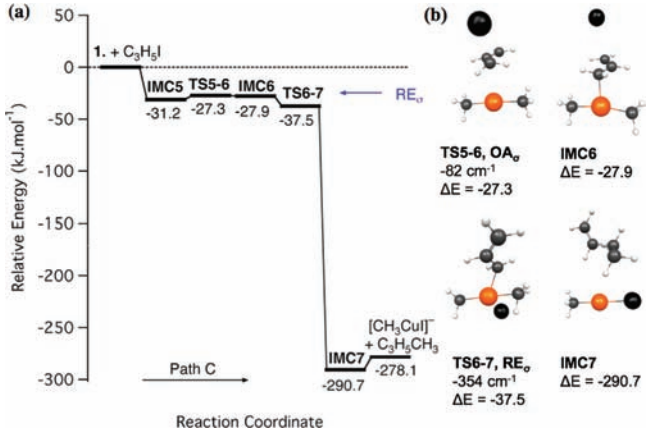

Figure 3. (a) Calculated B3LYP/Def2-QZVP//B3LYP/SDD6-31+G(d) relative energies (kJ mol^{-1}) for minima and transition states relevant to bimolecular reactions of $[CH_3CuCH_3]^-$ + C_3H_5I via path Cii (σ-oxidative addition). (b) Structures of minima and transition states relevant bimolecular reactions of $[CH_3CuCH_3]^-$ + C_3H_5I via path Cii of Scheme 5.

to the σ-oxidative addition pathway (barrier of −27.3 kJ mol^{-1}, Figure 3). This oxidative addition may be considered addition at the γ-carbon, although strictly the π-interaction involves both the β- and the γ-carbons. The copper complex is bent in the transition state (**TS8−9**, OA_π, Figure 4ci) to allow for this interaction. Because the formation of an η^3-allyl Cu(III) intermediate (**IMC9**, −92.2 kJ mol^{-1}) is thermodynamically favored over an η^1-allyl Cu(III) intermediate (**IMC6**, −27.9 kJ mol^{-1}), π-addition is the preferred pathway of oxidative addition. This η^3-allyl intermediate may undergo reductive elimination resulting in a cross-coupling product or homo-coupling product (Figure 4b). The theoretical prediction that the cross-coupling pathway is preferred (lower activation barrier of −45.4 kJ mol^{-1}, **TS9−10**) over the homo-coupling pathway (barrier of −30.0 kJ mol^{-1}, **TS9−12**) is consistent with the experimental observation that $[CH_3CuI]^-$ is formed in greater abundance than $[C_3H_5CuI]^-$ (Table 1).

dx.doi.org/10.1021/ja2069032 | J. Am. Chem.Soc. 2012, 134, 2569−2580

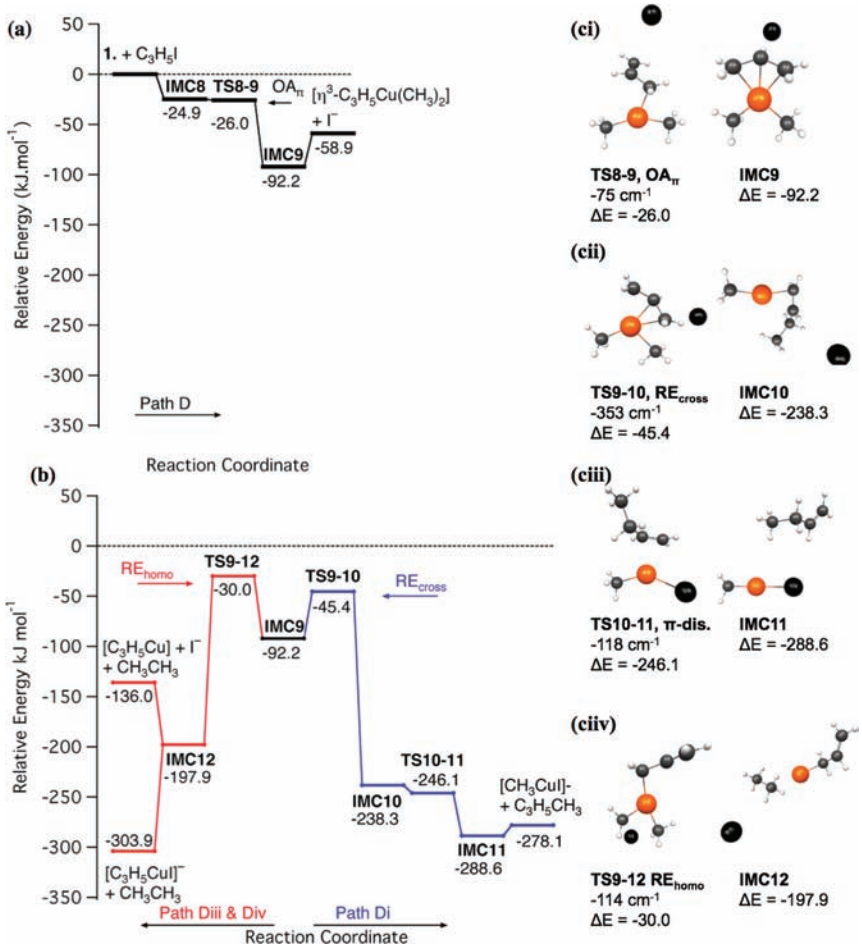

Figure 4. Calculated B3LYP/Def2-QZVP//B3LYP/SDD6-31+G(d) relative energies (kJ mol^{-1}) for minima and transition states relevant to bimolecular reactions of $[CH_3CuCH_3]^-$ + C_3H_5I via path D (π-addition) of Scheme 5. (a) π-Oxidative addition; (b) reductive elimination from the intermediate IMC9; blue line, path Di, cross-coupling; red line, paths Diii and Div, homo-coupling; and (c) structures of minima and transition states relevant bimolecular reactions of $[CH_3CuCH_3]^-$ + C_3H_5I via (i) path D, π-addition; (ii,iii) path Di, cross-coupling; and (iv) paths Diii and Div, homo-coupling.

As noted previously, the iodide anion can be a product of cross-coupling, homo-coupling (Scheme 4), or, more simply, oxidative addition (eqs 3 and 4). Calculations predict that while the S_N2 and oxidative addition/reductive elimination reactions are all thermodynamically viable (entry 1 of Tables 2 and 3), the kinetically and thermodynamically most preferred pathway for formation of I^- proceeds via the formation of the η^3-allyl intermediate.

Table 2. Calculated B3LYP/Def2-QZVP//B3LYP/SDD6-31+G(d) Energies (kJ mol^{-1}) for Concerted Nucleophilic Substitution of $[CH_3MCH_3]^-$ and C_3H_5I

	nucleophilic substitution		separated products
M	TS S_N2', path A	TS S_N2, path B	eqs 1 and 2
Cu	+11.4	+2.2	−278.1[a] (−127.4)[b]
Ag	+13.7	+4.9	−282.3[a] (−132.1)[b]
Au	+32.8	+23.5	−248.8[a] (−92.1)[b]

[a]Products $[CH_3MI]^-$ + $C_3H_5CH_3$. [b]The numbers in parentheses refer to products $[CH_3M]$ + $C_3H_5CH_3$ + I^-.

2.2. Comparative Reactivity of Coinage Metal Dimethylmetallates: M = Cu, Ag, and Au. Not only are the experimentally observed reaction rates of allyl iodide with dimethylargentate and dimethylaurate dramatically reduced relative to dimethylcuprate, but the types of ionic products formed vary (Table 1). Thus, the role of the metal center on the energetics associated with each of the mechanisms (Scheme 5) has been examined. Key data for all three metallates are summarized in Tables 2, 3, and 4, while the potential energy surfaces for $[CH_3AgCH_3]^-$ and $[CH_3AuCH_3]^-$ are given in the Supporting Information (Figure S3). These data are discussed in sections 2.3 and 2.4 in terms of the reactivities of dimethylargentate and dimethylaurate, respectively.

2.3. Dimethylargentate Reactivity. Table 2 compares the energies for paths A and B (Scheme 5). Because the transition state barriers for concerted nucleophilic substitution of dimethylargentate (entry 2, path A, +13.7 kJ mol^{-1}, path B, +4.9 kJ mol^{-1}) are very similar to those of dimethylcuprate (entry 1, path A, +11.4 kJ mol^{-1}, path B, +2.2 kJ mol^{-1}), the role of the metal is unimportant in these reactions. In contrast, both barriers for oxidative addition to the argentate via paths C and D (eqs 3 and 4, Scheme 5) are higher than those to the cuprate (Table 3). The σ-oxidative addition (eq 3, −2.0 kJ mol^{-1}) is preferred over the π-addition (eq 4, +13.0 kJ mol^{-1}), which contrasts with the cuprate where this trend is not observed (thermodynamically favoring formation of the η^3-allyl

dx.doi.org/10.1021/ja2069032 | J. Am. Chem.Soc. 2012, 134, 2569−2580

Table 3. Calculated B3LYP/Def2-QZVP//B3LYP/SDD6-31+G(d) Relative Energies (kJ mol^{-1}) for Oxidative Addition of $[CH_3MCH_3]^-$ and C_3H_5I

	oxidative addition		M(III) species	
M	TS OA_σ path C	TS OA_π path D	η^1-allyl (eq 3)	η^3-allyl (eq 4)
Cu	−27.3	−26.0	−27.9[a] (+6.3)[b]	−92.2[c] (−58.9)[d]
Ag	−2.0	+13.0	+3.1[a] (+47.8)[b]	−44.4[c] (−5.0)[d]
Au	−2.0	+6.5	−6.1[a] (+36.6)[b]	−54.8[c] (−22.5)[d]

[a]Ion−molecule complex $[\eta^1\text{-}C_3H_5M(CH_3)_2](I^-)$. [b]Separated products $[\eta^1\text{-}C_3H_5M(CH_3)_2] + I^-$. [c]Ion−molecule complex $[\eta^3\text{-}C_3H_5M(CH_3)_2](I^-)$. [d]Separated products $[\eta^3\text{-}C_3H_5M(CH_3)_2] + I^-$.

Table 4. Calculated B3LYP/Def2-QZVP//B3LYP/SDD6-31+G(d) Energies (kJ mol^{-1}) for Stepwise Oxidative Addition and Reductive Elimination of $[CH_3MCH_3]^-$ and C_3H_5I

				separated products			
	cross-coupling		homo-coupling	cross-coupling		homo-coupling	
M	TS RE_σ path Cii	TS RE_π path Dii	TS RE_π path Div	eq 6[a]	eq 5[b]	eq 8[c]	eq 7[d]
Cu	−37.5	−45.4	−30.0	−278.1	−127.4	−303.9	−136.0
Ag	+16.1	+12.4	+18.7	−282.3	−132.1	−307.0	−142.8
Au	+23.7	n/a	n/a	−248.8	−92.1	−265.2	−99.2

[a]Products $[CH_3MI]^-$ + $C_3H_5CH_3$. [b]Products $[CH_3M]$ + $C_3H_5CH_3$ + I^-. [c]Products $[C_3H_5MI]^-$ + CH_3CH_3. [d]Products $[C_3H_5M]$ + CH_3CH_3 + I^-.

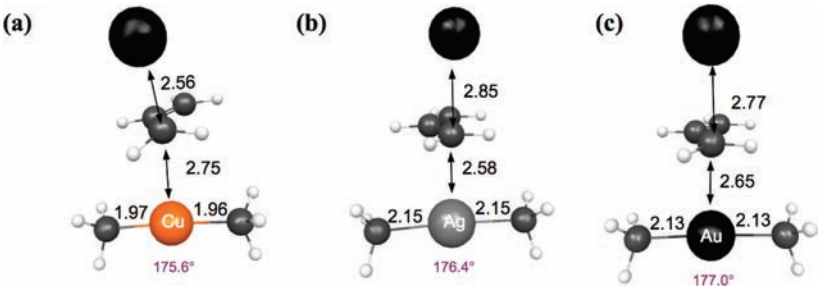

Figure 5. B3LYP/SDD6-31+G(d) optimized transition state geometries for σ-oxidative addition, $[CH_3MCH_3]^-$ with C_3H_5I, M = (a) Cu, (b) Ag, and (c) Au. Bond lengths are shown are in angstroms (Å).

intermediate). While formation of an η^3-allyl intermediate (−5.0 kJ mol^{-1}, Table 3) is thermodynamically favored over an η^1-allyl intermediate (prohibitive at +47.8 kJ mol^{-1}, Table 3), the kinetic barrier (OA_π, +13.0 kJ mol^{-1}) is higher in energy than that of the concerted reaction via path B. The RE mechanisms (paths C and D) via Ag(III) intermediates also suffer from kinetic barriers that are substantially higher in energy (+16.1, +12.4, and 18.7 kJ mol^{-1}; path C, Dii and Div, respectively, Table 4, eqs 5−8) than those from Cu(III) intermediates. Thus, OA/RE is not expected to be responsible for the experimentally observed product ions.

The experimental observation that dimethylargentate only reacts with allyl iodide via cross-coupling is nicely rationalized by the computational data. The most likely source of the product arising from cross-coupling, $[CH_3AgI]^-$, is via the S_N2 mechanism (path B, +4.9 kJ mol^{-1}). Thus, the argentate reaction is also predicted to be α-selective. Finally, the substantial difference in the experimentally observed kinetics of the reactions of allyl iodide with $[CH_3CuCH_3]^-$ and $[CH_3AgCH_3]^-$ (Table 1) can also be rationalized by the calculations. Because the nucleophilic substitution barrier via path B is predicted to be much higher in energy for the argentate than the rate-limiting steps in the cuprate cross-coupling reaction, the overall rate of reaction is expected to be slower.

2.4. Dimethylaurate Reactivity. In comparison to the cuprate and argentate, concerted nucleophilic substitution with the aurate is much higher in energy (Table 2, path A, +32.8 kJ mol^{-1}, path B, +23.5 kJ mol^{-1}) and thus should not occur under the experimental conditions of the ion trap. The higher barriers for dimethylaurate given in Table 2 likely arise from the relativistic shortening of Au−C bonds, as shown in Supporting Information Figure S4. The shortening of the gold bond lengths relative to copper and silver is observed for both the concerted S_N2 and S_N2' reaction TSs.

The barrier for σ-oxidative addition of allyl iodide to dimethylaurate (Table 3) resides slightly beneath the energy of the separated reactants (path C, −2.0 kJ mol^{-1}), and the π-oxidative addition barrier (path D, +6.5 kJ mol^{-1}) is only slightly above. This contrasts with the reaction energetics for copper, but parallels the preferences of silver for σ-oxidative addition. The trend for π-oxidative addition barrier matches the known trend in d-orbital energies (Cu ≫ Au > Ag), as discussed further below.

Despite the kinetic viability of oxidative addition, the resultant ion−molecule complexes are unable to undergo reductive elimination as the kinetic barrier is substantial (Table 4, path C, +23.7 kJ mol^{-1}) or the connecting transition state is completely absent (path D). This is consistent with previous predictions for reductive elimination from Au(III) intermediates.[7b,16d] Because there is no opportunity for homo-coupling or cross-coupling, the aurate is predicted to be unreactive in all C−C bond-forming reactions with allyl iodide.

dx.doi.org/10.1021/ja2069032 | J. Am. Chem.Soc. 2012, 134, 2569−2580

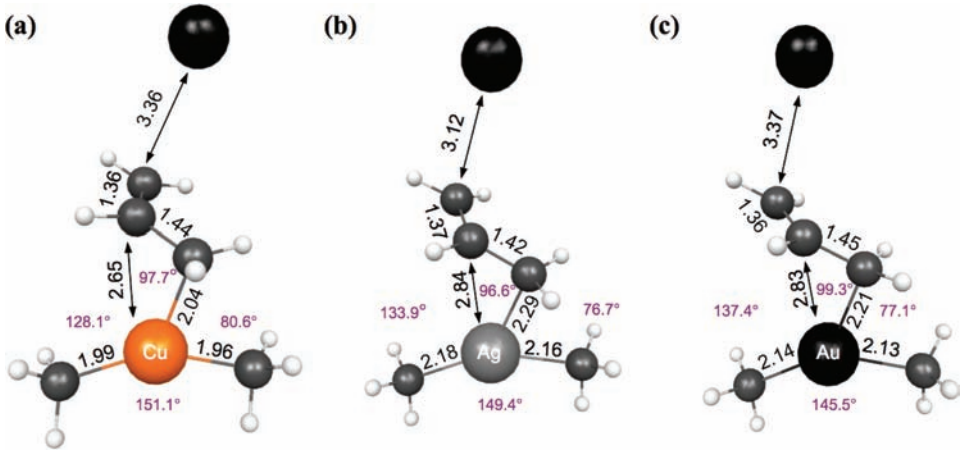

Figure 6. B3LYP/SDD6-31+G(d) optimized transition state geometries for π-addition of $[CH_3MCH_3]^-$ with C_3H_5I, M = (a) Cu, (b) Ag, and (c) Au. Bond lengths shown are in angstroms (Å).

The only kinetically and thermodynamically viable pathway is π-oxidative addition (+6.5 kJ mol^{-1}) with formation of I^- and an η^3-allyl intermediate (Table 1, −22.5 kJ mol^{-1}). This is consistent with the experimental observation of I^- as essentially the sole product (Supporting Information Figure S1c and Table 1). Because the rate-limiting step is much higher in energy than that of the cuprate reactions, the aurate is predicted to react more slowly with allyl iodide, consistent with the experimental observations.

2.5. Transition State Properties. The properties (structure and energy) of the transition states associated with oxidative addition and reductive elimination for $[CH_3MCH_3]^-$ (where M = Cu, Ag, and Au) are worthy of further comment. Figure 5 shows those associated with the σ-oxidative addition pathway. Inversion of the stereochemistry of the α-carbon center is consistent with the S_N2-like nature of the addition transition state. The degree of distortion from linearity of the metal complex follows the order: Cu (175.6°, Figure 5a) > Ag (176.4°, Figure 5b) > Au (177.0°, Figure 5c). This is the same order as that previously reported for the analogous reaction between $[CH_3MCH_3]^-$ and methyl iodide,[16d] although the M = Cu complex is less distorted in the case of methyl iodide. A possible reason for this is the increased steric hindrance at the reaction site.

The transition state vibration in Figure 5 is of the typical S_N2 variety, where the M−C bond is forming as the iodide leaves, combined with an inversion of the stereochemistry of the α-carbon. Only in Figure 5a is there an associated "twist" to this motion of the H atom, indicating some form of interaction between it and the copper center. The bond-forming molecular orbital for M = Cu is the HOMO (formed by σ-3d$_{z2}$), while that for M = Ag and Au is the HOMO−1 orbital (the HOMO having an antibonding interaction).

The π-oxidative addition transition state for each of the dimethylmetallates is shown in Figure 6. One of the most pronounced features is the change in energies relative to reactants: −26.0 kJ mol^{-1} for dimethylcuprate (Figure 6a); +13.0 and +6.5 kJ mol^{-1} for dimethylargentate and dimethylaurate, respectively (Figure 6b and c). This marked difference is a direct effect of the lower lying 4d and 5d orbitals of these latter two species. The transition states exhibit substantially more bending from linearity than those associated with the σ-oxidative addition pathway (Figure 5). Interestingly, the ordering of degree of distortion from linearity of the metal complex is reversed: Au (145.5°, Figure 6c) > Ag (149.4°, Figure 5b) > Cu (151.1°, Figure 6a). The deformation energy required of the metal complexes is more than that of the two reactions previously studied (σ-oxidative addition of allyl iodide and methyl iodide),[16d] due to the bending that is required of all three structures to expose the d orbitals suitable for π-interaction. The π-oxidative addition TS also requires a greater deformation energy associated with allyl iodide than does the σ-oxidation addition TS, because the C−I bonds in the former transition states are elongated (>3 Å for Cu, Ag, and Au; Figure 6) as compared to those in the latter transition states (<3 Å for Cu, Ag, and Au; Figure 5). These deformation energies should be well compensated by beneficial metal−carbon d−π^* interaction, particularly for the reaction of dimethylcuprate.

The TSs for reductive elimination from the M(III) species have been analyzed previously,[7b] but it is worth noting that the presence of an iodide anion assists these processes[42] by reducing the energetics associated with transition states, intermediates, and final products (Supporting Information Figures S8−11). To summarize, the TSs to cross-coupling via reductive elimination from either η^1-allyl or η^3-allyl Cu(III) intermediates are energetically viable, while from Ag(III) intermediates they are much higher in energy. For M = Cu and Ag, all of the cross-coupling TS RE geometries are a distorted T-shapes bearing iodide at the metal center. No reductive elimination is possible from the η^1-allyl Au(III) intermediate as the barrier for TS RE$_\sigma$ is prohibitively high; this is a Y-shaped TS where iodide is not interacting with the metal center. No TS geometry to reductive elimination from the η^3-allyl Au(III) complex is viable.

The homo-coupling pathway only occurs via the η^3-allyl intermediate, with the ligand opening up into a η^1-allyl product. While this path is kinetically viable for copper (−30 kJ mol^{-1}), this analogous barrier is too high for silver (+18.7 kJ mol^{-1}), and this process should not occur for dimethylaurate because no TS was found on the singlet surface.

2.6. Substrate Effects: Allyl Iodide versus Methyl Iodide. How does the allylic substrate influence the reactivity of dimethylmetallates in C−C bond-forming reactions? It is useful here to briefly compare the reactivity of allyl iodide with that of methyl iodide.[16,43] An obvious mechanistic difference is that paths A and D of Scheme 5 are not available for methyl iodide. Does the substrate influence the energetics associated with paths B and C? The overall trend for all three metals for path B

dx.doi.org/10.1021/ja2069032 | J. Am. Chem.Soc. 2012, 134, 2569−2580

(Scheme 5) is that there is essentially no difference in barrier between both substrates, a consequence of a similar hybridization of the carbon forming the bond in the S_N2-like transition state. For path C, the barrier associated with σ-oxidative addition to $[CH_3MCH_3]^-$ is also virtually the same for both substrates, as is the relative stability of the resultant M(III) intermediate. However, the kinetic barrier for reductive elimination is significantly lowered by the allylic substrate.

Because the barriers for paths B and D tended to be significantly lower than those of paths A and C, the allylic substrate exhibits increased reactivity (as compared to methyl iodide) in C−C bond-forming reactions of the cuprate and argentate. The stabilization of M(III) intermediates by the η^3-allyl ligand allows for the following: a lower energy reductive elimination pathway for the cuprate, when compared to that of the η^1-allyl ligand; the formation of the homo-coupling product, $[C_3H_5CuI]^-$; and the formation of a stable Au(III) intermediate.

CONCLUSIONS

Coinage metal-mediated C−C bond-coupling reactions are widely used in organic synthesis, and new variants continue to be actively explored. Yet remarkably little is known about how the nature of the metal center influences reactivity and mechanism. Here, the first gas-phase experimental comparisons of the reactions of allyl iodide with the dimethylmetallates, $[CH_3MCH_3]^-$, of the copper triad are reported. In addition, detailed density functional theory (DFT) calculations were carried out on a range of possible mechanisms (Scheme 5) for this important model of the prototypical, synthetically valuable "allylic alkylation" reaction.

Dimethylcuprate was found to be the superior reagent, reacting 3 orders of magnitude faster than dimethylargentate and dimethylaurate. Also, the types and yields of primary product ions detected via mass spectrometry differ for all three systems, suggesting a change of mechanism on moving down the group. Thus, for M = Cu, the following products were observed: (i) I^- (branching ratio = 75%); (ii) $[CH_3CuI]^-$ (branching ratio = 24%); and (iii) $[C_3H_5CuI]^-$ (branching ratio = 1%). When M = Ag, solely the cross-coupling product $[CH_3AgI]^-$ (branching ratio = 81%) is formed along with I^- (19%), while for M = Au, only I^- is detected, which can arise from oxidative addition.

As neutral product(s) are not detected in these gas-phase experiments, they cannot be used to differentiate between various mechanisms. Thus, DFT calculations play an important role in gaining insights into potential pathways that yield the observed product anions. For Cu, the energetically preferred mechanism involves oxidative addition and reductive elimination. This may occur competitively via two pathways: either via an η^3-allyl or via an η^1-allyl Cu(III) intermediate. However, the former path is the thermodynamically and kinetically preferred, due to stabilization of the Cu(III) intermediate and RE TS. A key finding is that both transition states for cross-coupling from the η^3-allyl and η^1-allyl Cu(III) intermediates are lower in energy than that for homo-coupling, which is consistent with the experimentally observed branching ratios for these product channels. In contrast, for M = Ag, the concerted nucleophilic substitution reaction at the S_N2 position is favored. This is consistent with the experimental observation that $[CH_3AgI]^-$ is detected but $[C_3H_5AgI]^-$ is not. Thus, reactions utilizing the argentate should be α-selective and are slowed by the comparatively high kinetic barrier to C−C bond formation. When M = Au, the predicted mechanism is oxidative addition to form an η^3-allyl Au(III) intermediate and iodide, in which the former is stable with respect to reductive elimination. Oxidative addition is thus consistent with the observation of I^- as the sole ionic product. Furthermore, the experimentally determined reactivity orders of $[CH_3CuCH_3]^- \gg [CH_3AgCH_3]^- \approx [CH_3AuCH_3]^-$ are consistent with the DFT calculations, which show higher barriers for the transition states associated with the key reaction pathways for $[CH_3AgCH_3]^-$ (path B, +4.9 kJ mol^{-1}) and $[CH_3AuCH_3]^-$ (π-oxidative addition, +6.5 kJ mol^{-1}) as compared to $[CH_3CuCH_3]^-$ (via both OA/RE pathways, with σ-oxidative addition, −27.3 kJ mol^{-1}, and π-oxidative addition, −26.0 kJ mol^{-1}).

The current and past work[16d,27] clearly shows that the reactions of $[CH_3MCH_3]^-$ are influenced by both the metal and the substrate. For example, $[CH_3CuCH_3]^-$ only reacts via cross-coupling when methyl iodide is the substrate, while homo-coupling also occurs when allyl iodide is the substrate, due to the involvement of the η^3-allyl Cu(III) intermediate. Because gas-phase decarboxylation reactions (eq 9) have provided a cornucopia of organometallic ions, $[RML_n]^{-/+}$,[44] the door is now open to detailed experimental and theoretical studies of the mechanisms of known and previously unexplored C−C bond-coupling reactions as a function of the properties of organometallic reagent ion (e.g., charge; nature of the metal, M; nature of the organic group, R; type of auxiliary ligand(s), L) and the organic substrate.

$$[RCO_2ML_n]^{-/+} \rightarrow [RML_n]^{-/+} + CO_2 \quad (9)$$

ASSOCIATED CONTENT

Supporting Information

Complete citation for ref 31. Branching ratio plots for $[CH_3CuCH_3]^-$ + C_3H_5I. Mass spectra for the ion−molecule reactions of $[CD_3CuCD_3]^-$, $[CH_3AgCH_3]^-$, and $[CH_3AuCH_3]^-$ with allyl iodide. Cartesian coordinates, imaginary frequencies, and energies (hartrees) for species relevant to each of the reaction pathways described in the text (Scheme 5, Figures 2−4, and Tables 2 and 3). Additional figures as mentioned in the text (comparison of transition states and potential energy surfaces). This material is available free of charge via the Internet at http://pubs.acs.org.

AUTHOR INFORMATION

Corresponding Author

rohair@unimelb.edu.au

ACKNOWLEDGMENTS

We thank the ARC for financial support via grant DP110103844 (to R.A.J.O.) and through the ARC CoE program. N.J.R. thanks (i) The University of Melbourne Faculty of Science for a Science Faculty Scholarship; (ii) The University of Melbourne for a Postgraduate Overseas Research Experience Scholarship (PORES) to travel to the University of Tokyo; and (iii) the Global COE Program for Chemistry Innovation (MEXT, Japan) for partial support of the research in Tokyo. The Victorian Partnership for Advanced Computing (VPAC) and the Chemical Sciences High Performance Computing Facility (Gomberg) are acknowledged for generous provision of computational resources.

REFERENCES

(1) For recent reviews, see: (a) Breit, B.; Demel, P. In *Modern Organocopper Chemistry*; Krause, N., Ed.; Wiley-VCH: Weinheim, Germany, 2002; Chapter 6, pp 210−223. (b) Sofia, A.; Karlstrom, E.; Backvall, J.-E. In *Modern Organocopper Chemistry*; Krause, N., Ed.; Wiley-VCH: Weinheim, Germany, 2002; Chapter 8, pp 261−283. (c) Spino, C. In *The Chemistry of Organocopper Compounds*; Rappoport, Z., Marek, I., Eds.; Wiley: Chichester, UK, 2009; Chapter 13, pp 603−691. (d) Alexakis, A.; Bäckvall, J. E.; Krause, N.; Pàmies, O.; Diéguez, M. *Chem. Rev.* **2008**, *108*, 2796−2823. (e) Harutyunyan, S. R.; den Hartog, T.; Geurts, K.; Minnaard, A. J.; Feringa, B. L. *Chem. Rev.* **2008**, *108*, 2824−2852. (f) Breit, B.; Schmidt, Y. *Chem. Rev.* **2008**, *108*, 2928−2951.

(2) Corey, E. J.; Posner, G. H. *J. Am. Chem. Soc.* **1967**, *89*, 3911−3912.

(3) Rona, P.; Tokes, L.; Tremble, J.; Crabbe, P. *J. Chem. Soc. D* **1969**, 43−44.

(4) (a) Pérez, M.; Fañanás-Mastral, M.; Bos, P. H.; Rudolph, A.; Harutyunyan, S. R.; Feringa, B. L. *Nat. Chem.* **2011**, *3*, 377−381. (b) Langlois, J.-B.; Alexakis, A. *Angew. Chem., Int. Ed.* **2011**, *50*, 1877−1881.

(5) (a) Geurts, K.; Fletcher, S. P.; Feringa, B. L. *J. Am. Chem. Soc.* **2006**, *128*, 15572−15573. (b) Tissot-Croset, K.; Alexakis, A. *Tetrahedron Lett.* **2004**, *45*, 7375−7378.

(6) For mechanistic reviews of organocuprate chemistry from a theoretical perspective, see: (a) Nakamura, E.; Mori, S. *Angew. Chem., Int. Ed.* **2000**, *39*, 3751−3771. (b) Nakamura, E.; Yoshikai, N. In *The Chemistry of Organocopper Compounds*; Rappoport, Z., Marek, I., Eds.; Wiley: Chichester, UK, 2009; Chapter 1, pp 1−21. (c) Mori, S.; Nakamura, E. *Modern Organocopper Chemistry*; Wiley-VCH: Weinheim, Germany, 2002; Chapter 10, pp 315−346. (d) Yoshikai, N.; Nakamura, E. *Chem. Rev.*, in press, DOI: 10.1021/cr200241f.

(7) (a) Yamanaka, M.; Kato, S.; Nakamura, E. *J. Am. Chem. Soc.* **2004**, *126*, 6287−6293. (b) Nakanishi, W.; Yamanaka, M.; Nakamura, E. *J. Am. Chem. Soc.* **2005**, *127*, 1446−1453. (c) Yamanaka, M.; Nakamura, E. *J. Am. Chem. Soc.* **2005**, *127*, 4697−4706. (d) Norinder, J.; Backvall, J.-E.; Yoshikai, N.; Nakamura, E. *Organometallics* **2006**, *25*, 2129−2132. (e) Yoshikai, N.; Zhang, S.-L.; Nakamura, E. *J. Am. Chem. Soc.* **2008**, *130*, 12862−12863.

(8) (a) Bartholomew, E. R.; Bertz, S. H.; Cope, S.; Murphy, M.; Ogle, C. A. *J. Am. Chem. Soc.* **2008**, *130*, 11244−11245. (b) Bartholomew, E. R.; Bertz, S. H.; Cope, S. K.; Murphy, M. D.; Ogle, C. A.; Thomas, A. A. *Chem. Commun.* **2010**, *46*, 1253−1254.

(9) (a) Weibel, J.-M.; Blanc, A.; Pale, P. In *Silver in Organic Chemistry*; Harmata, M., Ed.; John Wiley & Sons Inc.: Hoboken, NJ, 2010; Chapter 10, pp 285−328. (b) Stephen, A.; Hashimi, K. In *Silver in Organic Chemistry*; Harmata, M., Ed.; John Wiley & Sons Inc.: Hoboken, NJ, 2010; Chapter 12, pp 357−379. (c) Weibel, J.-M.; Blanc, A.; Pale, P. *Chem. Rev.* **2008**, *108*, 3149−3173. (d) Li, Z.; Brouwer, C.; He, C. *Chem. Rev.* **2008**, *108*, 3239−3265.

(10) One of the few examples in the literature involves C−C bond coupling between perfluoro isopropyl silver and allyl bromide: Dubot, G.; Mansuy, D.; Lecolier, S.; Normant, J. F. *J. Organomet. Chem.* **1972**, *42*, C105−106.

(11) For an excellent review on the gas-phase chemistry of coinage metals, see: Roithova, J.; Schröder, D. *Coord. Chem. Rev.* **2009**, *253*, 666−677.

(12) O'Hair, R. A. J. *Chem. Commun.* **2006**, 1469−1481.

(13) For a recent essay on the differences between gas-phase and solution-phase organometallic chemistry and their fruitful interplay, see: Agrawal, D.; Schröder, D. *Organometallics* **2011**, *30*, 32−35.

(14) There is a growing use of MS to monitor organometallic reactions. See: Santos, L. S., Ed. *Reactive Intermediates. MS Investigations in Solution*; Wiley-VCH: Weinheim, 2010.

(15) Gronert, S. *J. Am. Soc. Mass Spectrom.* **1998**, *9*, 845−848.

(16) (a) O'Hair, R. A. J. *Chem. Commun.* **2002**, 20−21. (b) Rijs, N.; Waters, T.; Khairallah, G. N.; O'Hair, R. A. J. *J. Am. Chem. Soc.* **2008**, *130*, 1069−1079. (c) Rijs, N. J.; O'Hair, R. A. J. *Organometallics* **2009**, *28*, 2684−2692. (d) Rijs, N. J.; Sanvido, G. B.; Khairallah, G. N.; O'Hair, R. A. J. *Dalton Trans.* **2010**, *39*, 8655−8662.

(17) (a) Rijs, N. J.; Yates, B. F.; O'Hair, R. A. J. *Chem.-Eur. J.* **2010**, *16*, 2674−2678. (b) Rijs, N. J.; O'Hair, R. A. J. *Organometallics* **2010**, *29*, 2282−2291.

(18) Taylor, R. J. K., Ed. *Organocopper Reagents: A Practical Approach*; Oxford University Press: Oxford, UK, 1994; pp 60−61.

(19) Busch, K. L.; Glish, G. L.; McLuckey, S. A. *Mass Spectrometry/Mass Spectrometry: Techniques and Applications of Tandem Mass Spectrometry*; VCH Publishers: New York, 1988.

(20) The rapid injection NMR technique has been used to highlight dramatic differences in the reactivity of organolithium clusters: (a) Jones, A. C.; Sanders, A. W.; Bevan, M. J.; Reich, H. J. *J. Am. Chem. Soc.* **2007**, *129*, 3492−3493. The elucidation of cuprate structures in solution continues to pose challenges: (b) Gschwind, R. M. *Chem. Rev.* **2008**, *108*, 3029−3053.

(21) For recent examples that highlight the role of clusters size in gas-phase ion−molecule reactions of mass-selected cluster ions of relevance to organometallic chemistry, see: (a) Wang, F. Q.; Khairallah, G. N.; O'Hair, R. A. J. *Int. J. Mass Spectrom.* **2009**, *283*, 17−25. (b) Khairallah, G. N.; Thum, C.; O'Hair, R. A. J. *Organometallics* **2009**, *28*, 5002−5011.

(22) Buchwald, S. L.; Bolm, C. *Angew. Chem., Int. Ed.* **2009**, *48*, 5586−5587 and references cited therein.

(23) There is an ongoing debate as to the precise role of gold in the Sonogashira coupling reaction: (a) González-Arellano, C.; Abad, A.; Corma, A.; García, H.; Iglesias, M.; Sánchez, F. *Angew. Chem., Int. Ed.* **2007**, *46*, 1536−1538. (b) Lauterbach, T.; Livendahl, M.; Rosellon, A.; Espinet, P.; Echavarren, A. M. *Org. Lett.* **2010**, *12*, 3006−3009. (c) Corma, A.; Juárez, R.; Boronat, B.; Sánchez, F.; Iglesias, M.; García, H. *Chem. Commun.* **2011**, *47*, 1446−1448.

(24) Decarboxylation has also been used to generate organometallics in solution. For reviews on the formation of organometallics, see: (a) Deacon, G. B. *Organomet. Chem. Rev., Sect. A* **1970**, *5*, 355−372. (b) Deacon, G. B.; Faulks, S. J.; Pain, G. N. *Adv. Organomet. Chem.* **1986**, *25*, 237−276. (c) Gooßen, L. J.; Collet, F.; Gooßen, K. *Isr. J. Chem.* **2010**, *50*, 617−629. For reviews on the use of catalytic decarboxylation reactions in synthesis, see: (d) Gooßen, L. J.; Gooßen, K.; Rodriguez, N.; Blanchot, M.; Linder, C.; Zimmermann, B. *Pure Appl. Chem.* **2008**, *80*, 1725−1733. (e) Gooßen, L. J.; Rodriguez, N.; Gooßen, K. *Angew. Chem., Int. Ed.* **2008**, *47*, 3100−3120. (f) Weaver, J. D.; Recio, A.; Grenning, A. J.; Tunge, J. A. *Chem. Rev.* **2011**, *111*, 1846−1913.

(25) For a recent demonstration of the reversibility of copper-catalyzed carboxylation/decarboxylation, see: Zhang, L.; Cheng, J.; Ohishi, T.; Hou, Z. *Angew. Chem., Int. Ed.* **2010**, *49*, 8670−8673.

(26) O'Hair, R. A. J. In *Reactive Intermediates. MS Investigations in Solution*; Santos, L. S., Ed.; Wiley-VCH: Weinheim, 2010; Chapter 6, pp 199−227.

(27) James, P. F.; O'Hair, R. A. J. *Org. Lett.* **2004**, *6*, 2761−2764.

(28) Khairallah, G. N.; Waters, T.; O'Hair, R. A. J. *Dalton Trans.* **2009**, *5*, 2832−2836.

(29) Waters, T.; O'Hair, R. A. J.; Wedd, A. G. *J. Am. Chem. Soc.* **2003**, *125*, 3384−3396.

(30) The accuracy of these ion trap rate measurements was checked by measuring the known rate constant for the reaction: $Br^- + CH_3I \rightarrow CH_3Br + I^-$, which has been determined at room temperature previously in a flowing afterglow apparatus: Gronert, S.; DePuy, C. H.; Bierbaum, V. M. *J. Am. Chem. Soc.* **1991**, *113*, 4009−4010. This rate was measured on the same day as each of the rate measurements for the reactions of allyl iodide with $[CH_3CuCH_3]^-$, $[CH_3AgCH_3]^-$, and $[CH_3AuCH_3]^-$. The previously reported $[CH_3CuCH_3]^- + CH_3I$ rate constant (ref 27) was also remeasured. In all cases, the rate constants were reproduced within error limits. This close agreement shows that the ion trap provides reproducible ion−molecule rate constants of near thermal ions, consistent with Gronert's equilibrium measurements, which have shown that ions within the ion trap are essentially at room temperature (see ref 15).

(31) Frisch, M. J.; et al. *Gaussian 03*; Gaussian, Inc.: Pittsburgh, PA, 2003.
(32) (a) Becke, A. D. *J. Chem. Phys.* **1993**, *98*, 5648−5652. (b) Lee, C.; Yang, W.; Parr, R. G. *Phys. Rev. B: Condens. Matter* **1988**, *37*, 785−789.
(33) (a) Dolg, M.; Wedig, U.; Stoll, H.; Preuss, H. *J. Chem. Phys.* **1987**, *86*, 866−872. (b) Hariharan, P. C.; Pople, J. A. *Theor. Chim. Acta* **1973**, *28*, 213−222. (c) Clark, T.; Chandrasekhar, J.; Schleyer, P. V. R. *J. Comput. Chem.* **1983**, *4*, 294−301. (d) Krishnan, R.; Binkley, J. S.; Seeger, R.; Pople, J. A. *J. Chem. Phys.* **1980**, *72*, 650−654. (e) Gill, P. M. W.; Johnson, B. G.; Pople, J. A.; Frisch, M. J. *Chem. Phys. Lett.* **1992**, *197*, 499−505.
(34) A detailed benchmarking study on cuprates has shown that the B3LYP method gives reaction energies qualitatively similar to the computationally expensive CCSD(T) method. See: Yamanaka, M.; Inagaki, A.; Nakamura, E. *J. Comput. Chem.* **2003**, *24*, 1401−1409.
(35) Although the structures and relative energies of loosely bound ion−molecule complexes (IMCs) are included here for completeness, the effectiveness of B3LYP in accurately predicting their properties was not assessed, and they should therefore be treated with caution. However, these pre- and postcomplexes do not influence the mechanistic conclusions drawn.
(36) (a) Weigend, F.; Ahlrichs, R. *Phys. Chem. Chem. Phys.* **2005**, *7*, 3297−3305. (b) Weigend, F.; Furche, F.; Ahlrichs, R. *J. Chem. Phys.* **2003**, *119*, 12753−12762. (c) Andrae, D.; Haeussermann, U.; Dolg, M.; Stoll, H.; Preuss, H. *Theor. Chim. Acta* **1990**, *77*, 123−141. Basis sets were obtained from the EMSL Basis Set Library via the Basis Set Exchange: (d) Schuchardt, K. L.; Didier, B. T.; Elsethagen, T.; Sun, L.; Gurumoorthi, V.; Chase, J.; Li, J.; Windus, T. L. *J. Chem. Inf. Model.* **2007**, *47*, 1045−1052.
(37) (a) Zhao, Y.; Truhlar, D. G. *Theor. Chem. Acc.* **2008**, *120*, 215−241. (b) Grimme, S. *J. Chem. Phys.* **2006**, *124*, 034108. (c) Schwabe, T.; Grimme, S. *Phys. Chem. Chem. Phys.* **2007**, *9*, 3397−3406.
(38) Bode, B. M.; Gordon, M. S. *J. Mol. Graphics Modell.* **1998**, *16*, 133−138.
(39) (a) Su, T.; Bowers, M. T. *Int. J. Mass Spectrom. Ion Phys.* **1973**, *12*, 347−356. (b) Lim, K. F. *Quantum Chem. Program Exch.* **1994**, *14*, 3.
(40) A reviewer has correctly pointed out that a detailed understanding of these kinetic isotope effects requires a comprehensive analysis of all of the competing reactions shown in Scheme 5. Because these ion trap mass spectrometry experiments do not detect neutrals, the isotope effects associated with all of these competing reactions cannot be measured. For discussions of isotope effects in mass spectrometry experiments, see: (a) Derrick, P. J. *Mass Spectrom. Rev.* **1983**, *2*, 285−298. (b) Lehman, T. A. *Mass Spectrom. Rev.* **1995**, *14*, 353−382. For a review on extreme kinetic isotope effects caused by reaction branching, see: (c) Thibblin, A.; Ahlberg, P. *Chem. Soc. Rev.* **1989**, *18*, 209−224.
(41) No reliable secondary KIE could be calculated in the reaction of $[CD_3AgCH_3]^-$ with allyl iodide for the following reasons: (1) the slow rate provided insufficient yields of product ions $[CD_3AgI]^-$ and $[CH_3AgI]^-$, and (2) the precursor silver carboxylate anions were depleted in esterification reactions involving C−O bond formation, $[CH_3CO_2AgL]^- + CH_2{=}CHCH_2I \rightarrow [IAgL]^- + CH_3CO_2CH_2CH{=}CH_2$ (where L = CH_3CO_2 and CH_3). For related esterification reactions between the silver acetate cation, $[CH_3CO_2Ag_2]^+$, and allyl iodide, see: Khairallah, G. N.; Waters, T.; O'Hair, R. A. J. *Eur. J. Mass Spectrom.* **2007**, *13*, 367−372.
(42) For a review on iodide effects in transition metal-catalyzed reactions, see: (a) Maitlis, P. M.; Haynes, A.; James, B. R.; Catellani, M.; Chiusoli, G. P. *Dalton Trans.* **2004**, 3409−3419. For a discussion of halide effects on stoichiometric metal-mediated reactions, see: (b) Fagnou, K.; Lautens, M. *Angew. Chem., Int. Ed.* **2002**, *41*, 26−47.
(43) The calculated data (E_0) in ref 16d are at the B3LYP/SDD6-31+G(d) level of theory, while those presented in Figures 2−4 and Tables 2−4 are at the B3LYP/Def2-QZVP//B3LYP/SDD6-31+G(d). Supporting Information Table S5 directly compares the energetics for both methyl iodide and allyl iodide substrates at the B3LYP/SDD6-31+G(d) level of theory.
(44) These include organomagnesates and organomagnesium cations, see: (a) O'Hair, R. A. J.; Vrkic, A. K.; James, P. F. *J. Am. Chem. Soc.* **2004**, *126*, 12173−12183. (b) Jacob, A. P.; James, P. F.; O'Hair, R. A. J. *Int. J. Mass Spectrom.* **2006**, *255*−*256*, 45−52. (c) Thum, C. C. L.; Khairallah, G. N.; O'Hair, R. A. J. *Angew. Chem., Int. Ed.* **2008**, *48*, 9118−9121. (d) Khairallah, G. N.; Thum, C.; O'Hair, R. A. J. *Organometallics* **2009**, *28*, 5002−5011. (e) Khairallah, G. N.; Yoo, E. J. H.; O'Hair, R. A. J. *Organometallics* **2010**, *29*, 1238−1245. (f) Leeming, M. G.; Khairallah, G. N.; da Silva, G.; O'Hair, R. A. J. *Organometallics* **2011**, *30*, 4297−4307. For organonickel, palladium, and platinum cations, see: (g) Woolley, M.; Khairallah, G. N.; Donnely, P. S.; O'Hair, R. A. J. *Rapid Commun. Mass Spectrom.* **2011**, *25*, 2083−2088.

■ NOTE ADDED IN PROOF

The formation and gas phase fragmentation reactions of tetralkylcuprates has been recently published: Putau, A.; Brand, H.; Koszinowski, K. *J. Am. Chem. Soc.* **2012**, *134*, 613−622.